A Rechargeable Liquid Metal-CO$_2$ Battery for Energy Storage and CO$_2$ Reduction to Carbon

Jan Gabski, Xinhui Sun, Landysh Iskhakova, Junhang Dong [*]

Department of Chemical and Environmental Engineering, University of Cincinnati, Cincinnati, OH 45221, USA.

[*] Corresponding author: dongj@ucmail.uc.edu (J.D.)

Supplemental Information

Fig. S1: (a) SEM image showing the cross-section of the porous α-alumina disc with large open pores before loading MCE, (b) SEM image showing the cross-section of the porous α-alumina disc after loading the $Li_{0.62}K_{0.38}CO_3$ MCE, and (c) SEM image and EDS elemental survey over the MCE-loaded alumina disc cross-section indicating that the porosity was fully filled by the MCE.
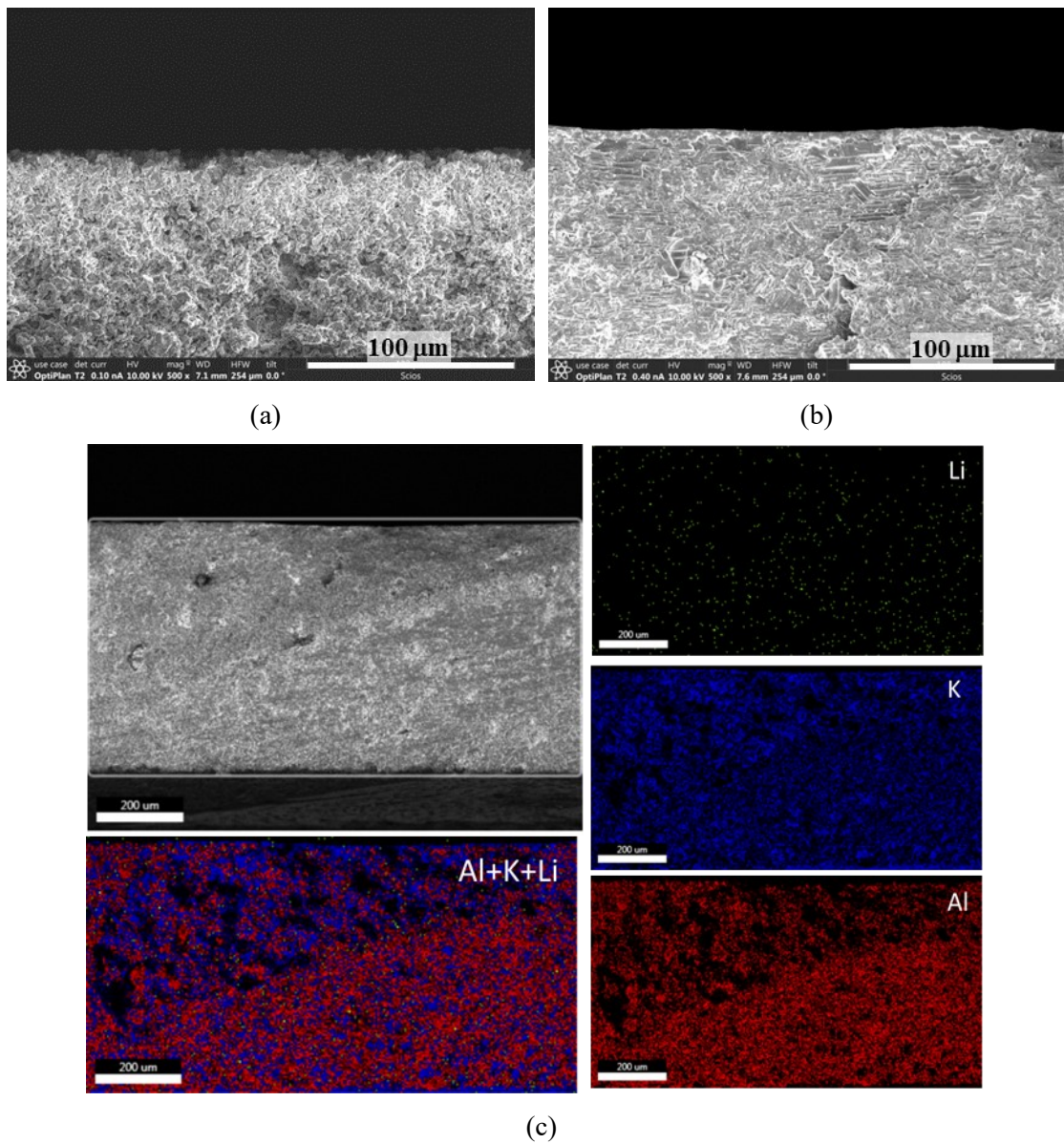

(a)

(b)

(c)

Fig. S2: (a) SEM image and EDS elemental survey of the fresh Ni foam indicating no NiO films before oxidation in the CO_2/air stream at 508°C, (b) SEM and EDS elemental survey for the Ni foam after oxidation in the CO_2/air (30:70) flow at 508°C (6 – 7 h for loading the MCE and LGa and 4 h of operation) revealing a thick NiO film formed on the Ni metal that caused dramatic changes in surface morphology and textures, and (c) XRD spectra of the Ni foam before and after surface oxidation under LGaCB operation conditions confirming the structure of NiO film coated Ni metal (NiO/Ni) for the NiGE.
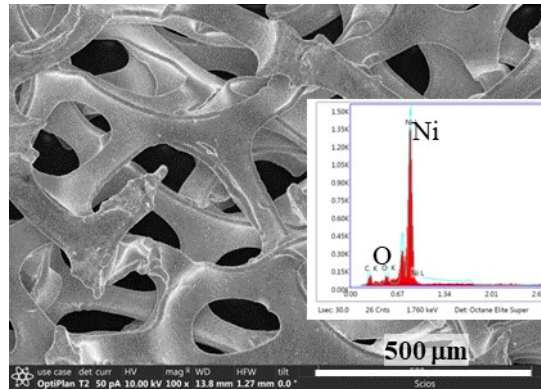

(a)
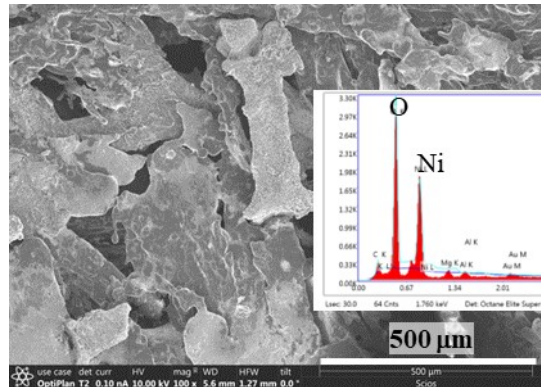
(b)
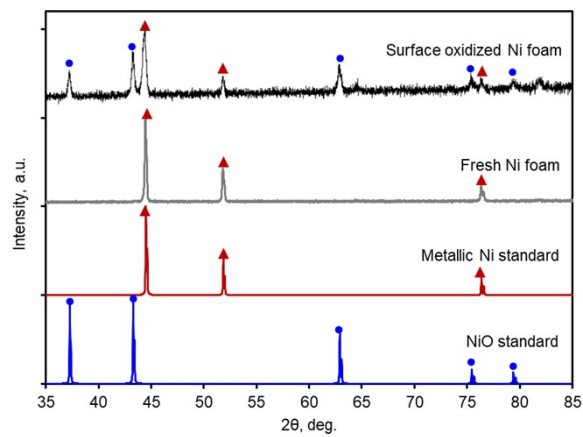
(c)

Fig. S3: (a) EIS measured ASR (~ 2.7 $\Omega \cdot cm^2$) and conductivity σ_{MCE} (~0.11 S·cm^{-1}) of the MCE-loaded alumina disc before loading LGa (stabilized ASR ~ 1.0 $\Omega \cdot cm^2$ and (b) ASR of the LGaCB (LGa-loaded) cell as a function of stabilizing time at 508±3°C. The LGaCB MEA ASR increased from ~ 1.0 to ~ 21 $\Omega \cdot cm^2$ in the first 30 min and then decreased and stabilized at ~ 2.7 $\Omega \cdot cm^2$ in the next 35 min. This temporal evolution of cell ASR was likely caused by the formation and accumulation of Ga oxides at the LGa/MCE interface under the open circuit MR mode. Under the MR mode, LGa reacted with CO_2 permeated from the NiGE CO_2 feed side through the MCE that generated Ga_2O_3 and carbon. These electrically resistive solid products accumulated to a certain level at which the solid agglomerates were buoyed to the surface of LGa, which is heavier than both solids. The ASR was stabilized after the deposition and dispersion of the solid products reached a steady state.
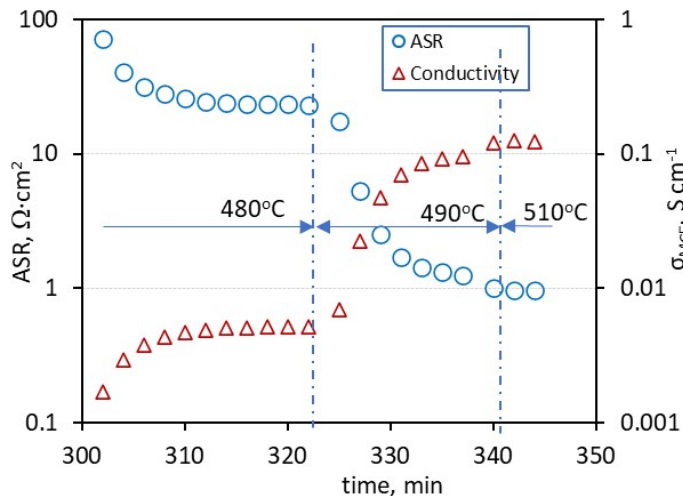

(a)
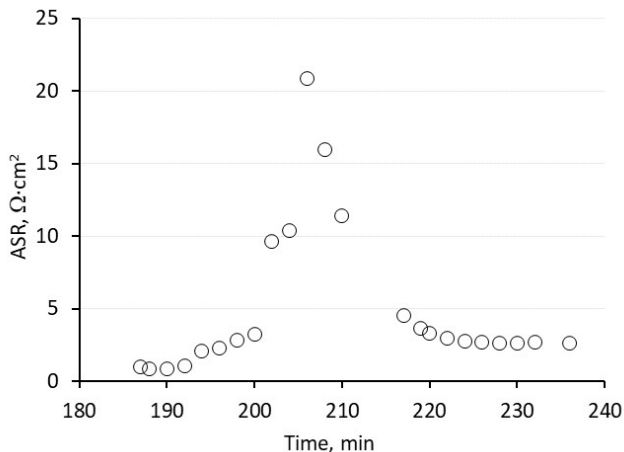
(b)

Fig. S4: Characterization of the LGa surface samples from the LGaCB after running in open-circuit MR mode: (a) SEM and EDS results showing needle-shaped and spherical nanoparticles (dia. <20 nm) of Ga oxides. The EDS showed an O/Ga atomic ratio of 1.63 for the particles, which agreed well with value of 1.5 for Ga_2O_3; (b) the Raman shift spectra indicating carbon products in graphitic phase. Strong peaks of Ga oxides were observed together with a weak peak at ~ 260 cm^{-1} for solid Ga, which could exist at room temperature. Liquid Ga does not have Raman peaks; and (c) XPS spectra showing substantial changes in Ga oxidation states after MR mode operation. The Ga 2p XPS peak shift towards high binding energy (1147 eV) indicated an increasing Ga^{3+}/Ga ratio in the LGa. [3] The appearance of C=O and C-O peaks indicate surface oxidation of graphite products but peaks of carbonates (O-C=O binding energy at ~289.5 eV [1]) were not appreciable.
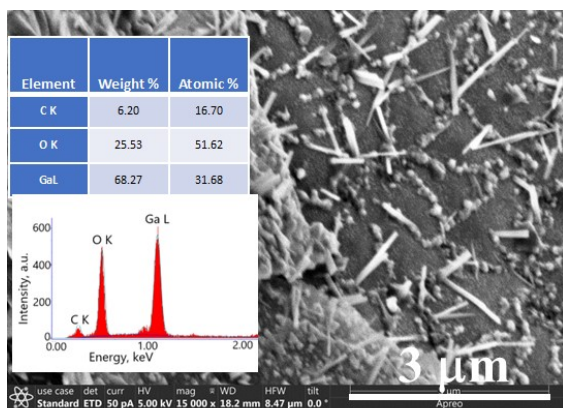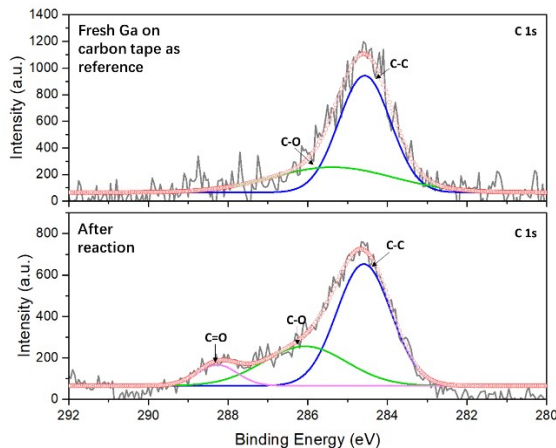

(a)
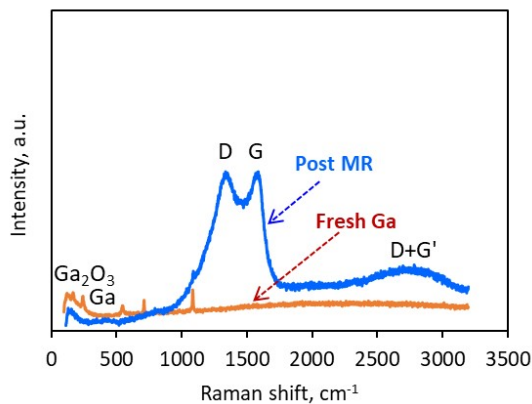
(b)
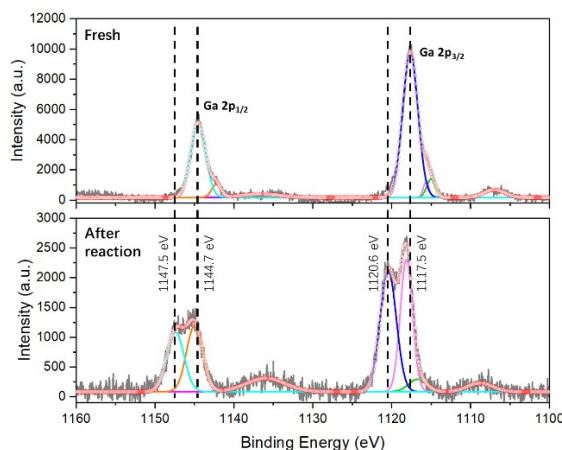
(c)

(d)

Fig. S5: (a) SEM-EDS observations of the Ga surface after fired at 508°C in air for 2 h. The Ga oxide particles appeared to be large agglomerates of nanoparticles with primary grain sizes ~ 50 nm; and (b) SEM-EDS observations of the Ga surface after being exposed to a 30%CO$_2$/70%N$_2$ mixture flow at 508°C for 2 h. The Ga oxide particles were also large agglomerates of nanoparticles with primary grain sizes ~ 30 nm. Carbon was not noticeable based on the EDS peaks of carbon which was almost the same as the background level (measured for bear Al sample holder). The diminishing carbon in the LGa treated in 30:70 CO$_2$/N$_2$ mixture was likely caused by significant reverse CO disproportionation ($2CO \leftrightarrow CO_2 + C$) in the CO$_2$-rich environment during high temperature Ga-catalyzed CO$_2$RC [2].
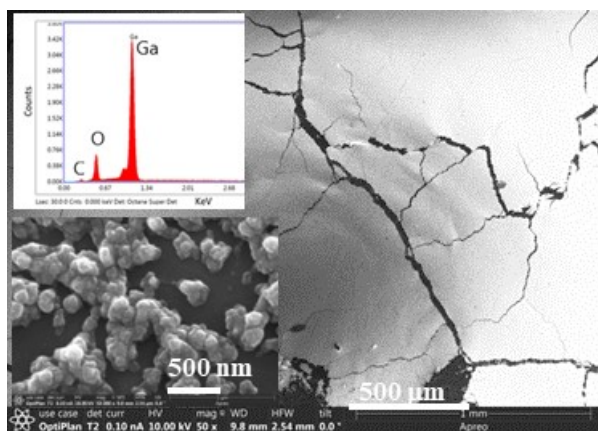

(a)
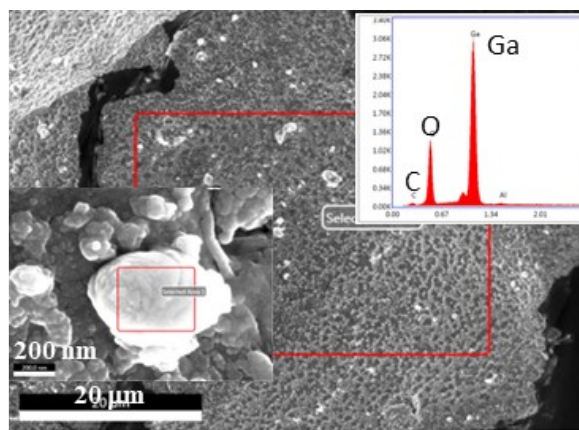
(b)

Fig. S6: Direct tests of the LGaCB after the 4-h heating-up and open-circuit stabilization period: (a) The open circuit voltage (OCV) measured after ASR stabilized at ~ 2.7 $\Omega \cdot cm^2$. The OCV (0.62±0.15 V) was far below the E_r^o; (b) the polarization curve and $P_e \sim i_{dch}$ dependency, suggesting that the interfaces in the MEA were severely contaminated; and (c) V_{dch} as a function of time at low i_{dch}. The small V_{dch} at very low i_{dch} indicate large losses.
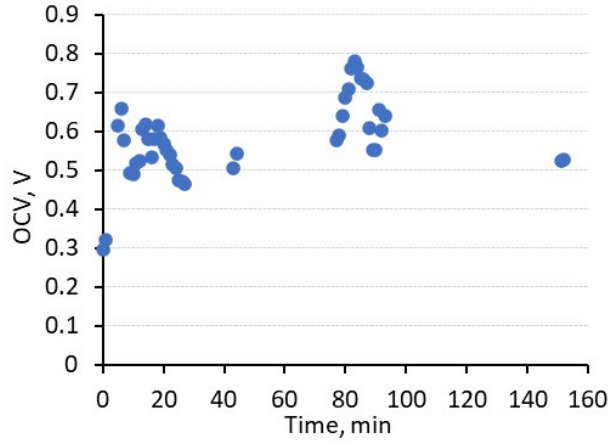
(a)
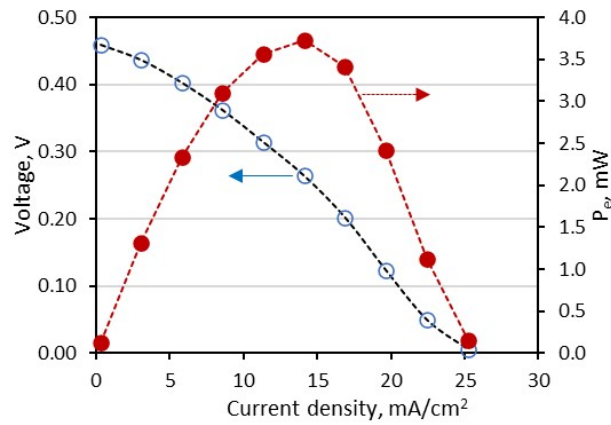
(b)
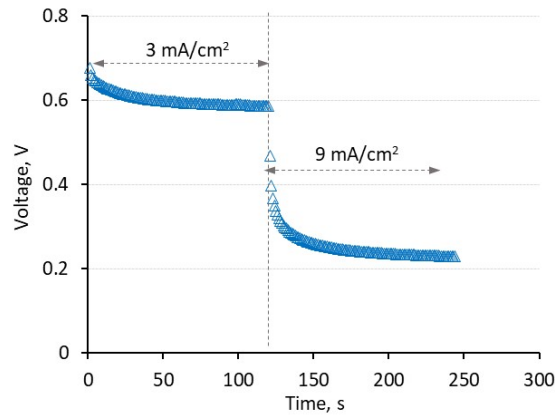
(c)

Fig. S7: Comparisons of the i_{dch}-dependent V_{dch}, and P_e between the LGaCB and existing MCBs (open symbols represent $\eta_{d/ch}$ and closed symbols represent P_e: ◊♦ LiCB [4]; □■ NaCB [5]; ○● ZnCB [6-10]; △▲ LGaCB of this work).
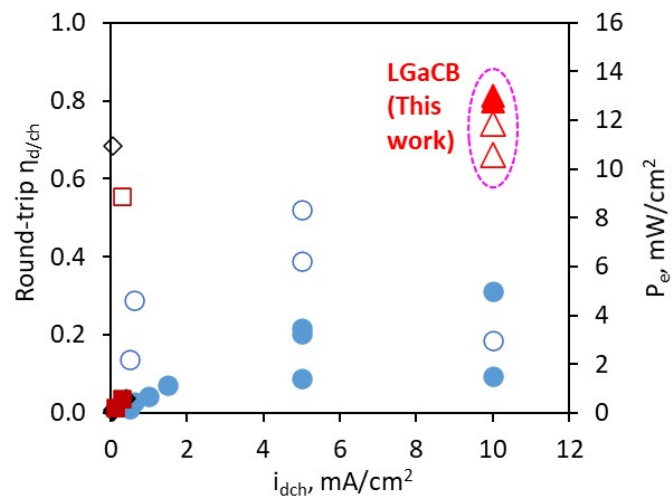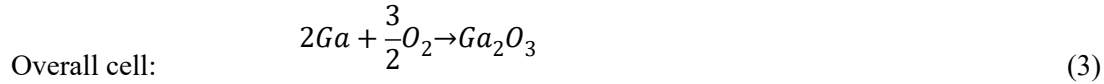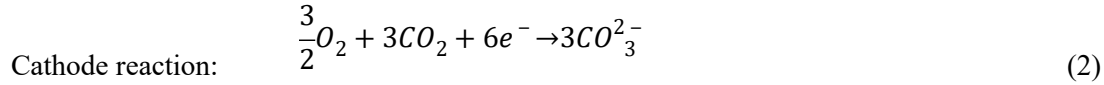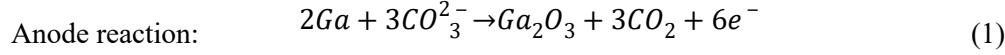
Note: Estimate of E_r and ΔV_a of LGaCB

The electrochemical reactions in the LGaCB are:

Anode reaction:
$$2Ga + 3CO_3^{2-} \rightarrow Ga_2O_3 + 3CO_2 + 6e^- \tag{1}$$

Cathode reaction:
$$\frac{3}{2}O_2 + 3CO_2 + 6e^- \rightarrow 3CO_3^{2-} \tag{2}$$

Overall cell:
$$2Ga + \frac{3}{2}O_2 \rightarrow Ga_2O_3 \tag{3}$$

The feed of 30%CO_2 + 70%air at a flowrate of 20 cm³ (STP)/min provided CO_2 and O_2 in large excess of needs for the current densities 10 and 30 mA/cm², and therefore, the O_2 and CO_2 partial pressures, i.e., P_{O_2} and P_{CO_2}, were almost unchanged in the NiGE cathode side, i.e., $P_{O_2,C} \approx 0.150\ bar$ and $P_{CO_2,C} \approx 0.304\ bar$. For ideal gases behavior, the activity of a gas component $i\ (= O_2$ and $CO_2)$, are given by $a_i = P_i/P_o$, where reference $P_o = 1\ bar$. The CO_2 from anodic reaction (1) is conceivably in chemisorbed state on LGa, and thus $a_{CO_2} \approx 1$ in the LGaA. The E_r under the operation conditions can be estimated by the Nernst equation as following using an approximation of constant $\Delta s_{r,T} = \Delta s_{r,298}$:

$$E_r = E_{r,298}^o + \frac{\Delta s_r}{6F}(T - T_o) + \frac{RT}{2F}\ln\left(P_{O_2,C}^{0.5} \cdot P_{CO_2,C}\right) = 1.400\ V \tag{4}$$

The thermodynamics properties for Ga_2O_3 formation are obtained from reference [11]: $\Delta H_{r,298}^o = -1089.1$ kJ/mol, $\Delta G_{r,298}^o = -998.3$ kJ/mol, and $\Delta s_{r,298}^o = (\Delta H_{r,298}^o - \Delta G_{r,298}^o)/298.15 = -304.5$ kJ/mol·K. The standard reversible LGaCB cell potential, $E_{r,298}^o$, is obtained at T = 298.15°C and all gas partial pressures at 1 bar:

$$E_{r,298}^o = \frac{-\Delta G_{r,298}^o}{nF} = 1.72\ V \tag{5}$$

The LGaCB cell ASR obtained from the linear segment of the last polarization curve in Fig. 3c is ~15.5 Ω·cm² and the mass transport overpotential $\Delta V_m \approx 0\ V$ when $i_{dch} \ll i_L$ (where the current limit $i_L \approx 122$ mA/cm², Fig. 3b). Thus, the reaction (kinetic) overpotential ΔV_a at $i_{dch} = 10$ mA/cm² and a stabilized $V_{dch} = 1.235$ V is obtained by:

$$\Delta V_a = E_r - V_{dch} - i_{dch} \cdot ASR = 0.008\ V \tag{6}$$

References:

1. Dedryvere, R., L. Gireaud, S. Grugeon, S. Laruelle, J.-M. Tarascon, D. Gonbeau, Characterization of Lithium Alkyl Carbonates by X-ray Photoelectron Spectroscopy: Experimental and Theoretical Study. *J. Phys. Chem. B,* 2005, **109**, 15868-15875.

2. Zuraiqi, K., A. Zavabeti, J. Clarke-Hannaford, B.J. Murdoch, K. Shah, M.J.S. Spencer, C.F. McConville, T. Daeneke, K. Chiang, Direct conversion of CO_2 to solid carbon by Ga-based liquid metals. *Energy Environ. Sci.,* 2022, **15**, 595-600.

3. Rodríguez, C.I.M., M.A.L. Álvarez, J.J.F Rivera, G.G.C. Arízaga, C.R. Michel, α-Ga_2O_3 as a Photocatalyst in the Degradation of Malachite Green. *ECS J. Solid State Sci. Techn.,* 2019, **8**(7) Q3180-Q3186.

4. Y. Xing, Y. Yang, D. Li, M. Luo, N. Chen, Y. Ye, J. Qian, L. Li, D. Yang, F. Wu, R. Chen, S. Guo, *Adv. Mater.,* 2018, **30**, 1803124.

5. X. Hu, Z. Li, Y. Zhao, J. Sun, Q. Zhao, J. Wang, Z. Tao, J. Chen, *Sci. Adv.,* 2017, **3**, e1602396.

6. R. Yang, J. Xie, Q. Liu, Y. Huang, J. Lv, M.A. Ghausi, X. Wang, Z. Peng, M. Wu,Y. Wang, *J. Mater. Chem. A,* 2019, **7**, 2575–2580.

7. J. Xie, X. Wang, J. Lv, Y. Huang, M. Wu, Y. Wang, J. Yao, *Angew. Chem. Int. Ed.,* 2018, **57**, 16996 –17001.

8. M. Yang, S. Liu, J. Sun, M. Jin, R. Fu, S. Zhang, H. Li, Z. Sun, J. Luo, X. Liu, *Appl. Catal. B: Environ.,* 2022, **307**, 121145.

9. S. Kaur, M. Kumar, D. Gupta, P.P. Mohanty, T. Das, S. Chakraborty, R. Ahuja, T.C. Nagaiah, *Nano Energy,* 2023, **109**, 108242.

10. H. Xie, H. Liao, S. Zhai, T. Liu, Y. Wu, F. Wang, J. Li, Y. Zhang, B. Chen, *Energy,* 2023, **263**, 125688.

11. W. M. Haynes, ed. (2011). CRC Handbook of Chemistry and Physics (92nd ed.). Boca Raton, FL, CRC Press. 2011, p. 5.12.